Brain tissue discovery and classification in HSI

Part of European project Helicoid
joint work with Stanciulescu B. & Angulo J.

B Ravi Kiran

Université Lille 3

beedotkiran@gmail.com

April 2, 2017

Plan

Problem description

HSI imaging for inter-operative visualization aid brain tumor removal

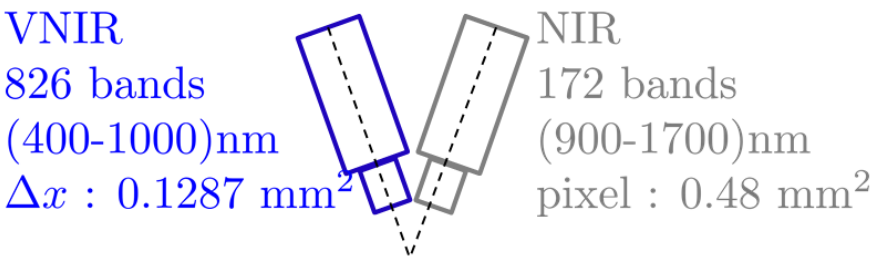

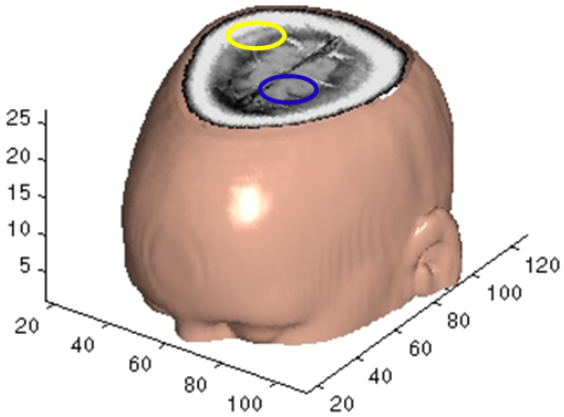

- 21 operations, VNIR & NIR images, 4-6 images / op.
- In-vivo cubes of brain tissue (tumor in view during surgery)
- Ex-vivo images of tumor.
- Plastic rings in each In-vivo image show locations containing *possible* tumor and healthy tissue.
- Tissue samples within markers are verified by pathology to confirm presence of tumor.

Outputs and Problems

Outputs Expected:

- Segment hyper-spectral images to detect tumor pixels and validate with ring markers.
- Visualization of brain tissue structure as interoperative aid
- Extract spectral signature of tumor tissues

Issues:

- **No labels/ground truth nor meta data about tumors.**
- Varying lighting, push-broom sensor vibrations.
- Varying tumor spectrum across patients and tumor types.
- Specular reflections prominent in many images.

In-vivo and Ex-vivo Images

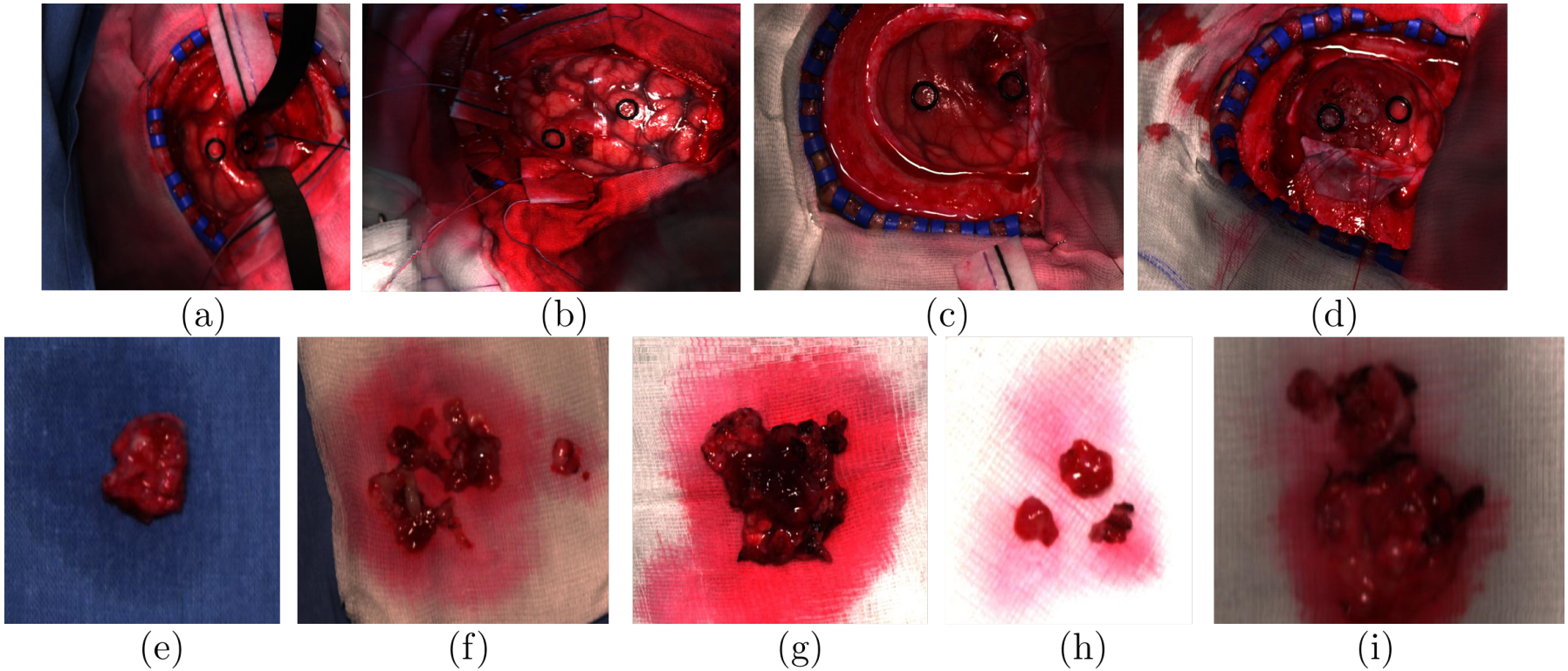

Figure : Two sets of HSI images (shown in RGB) captured during operation. The first row (a-d) consist of images taken during a surgical procedure before the extraction of tumor. The second row (e-i) consists of images taken after the extraction of the tumor. The resected tumor is placed on a cotton tissue and is captured again by the VNIR camera. (e-i) images serve as a weak ground truth, that ensure us tumor tissue in a localized window.

Overview

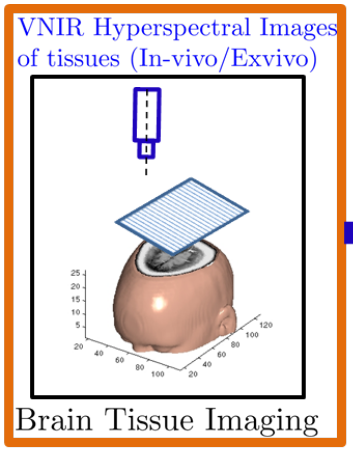

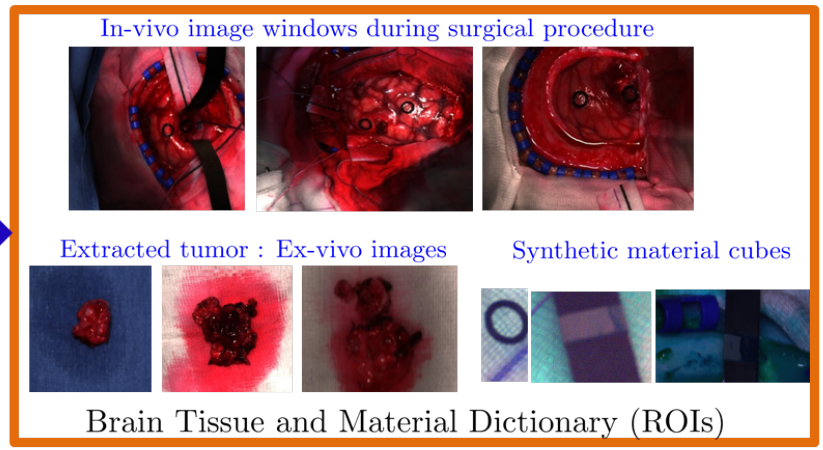

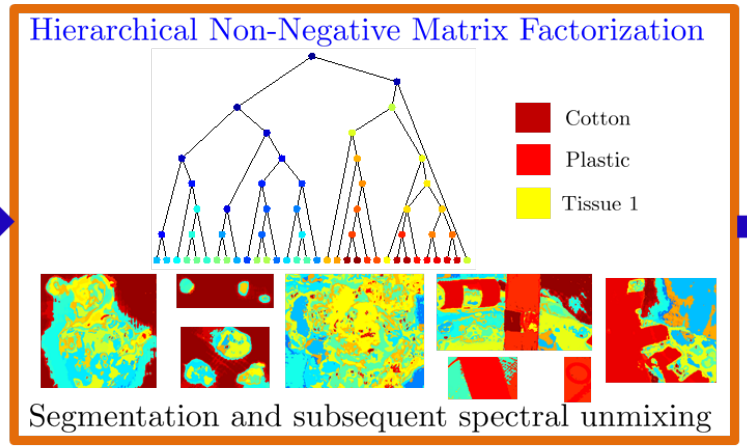

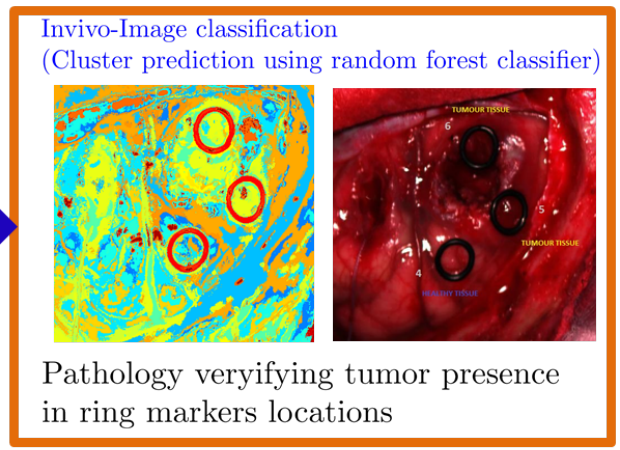

$X = \{I_i\} \bigcup \{E_j\}$
$X = X_{\text{train}} \cup X_{\text{test}}$
$X_{\text{train}} \cap X_{\text{test}} = \emptyset$

→ **CLUSTERING:** $y_{\text{train}} = C_k = \text{H2NMF}(X_{\text{train}})$

→ **VISUAL IDENTIFICATION** Tissue1, Tissue2, blood cotton, plastic, strap

→ **RANDOM FOREST TRAINING:** $F : X_{\text{train}} \rightarrow C_k$

→ **PREDICTION:** $y_{\text{test}} = F(X_{\text{test}})$ over unseen operations

Linear Mixing Model [10], [9]

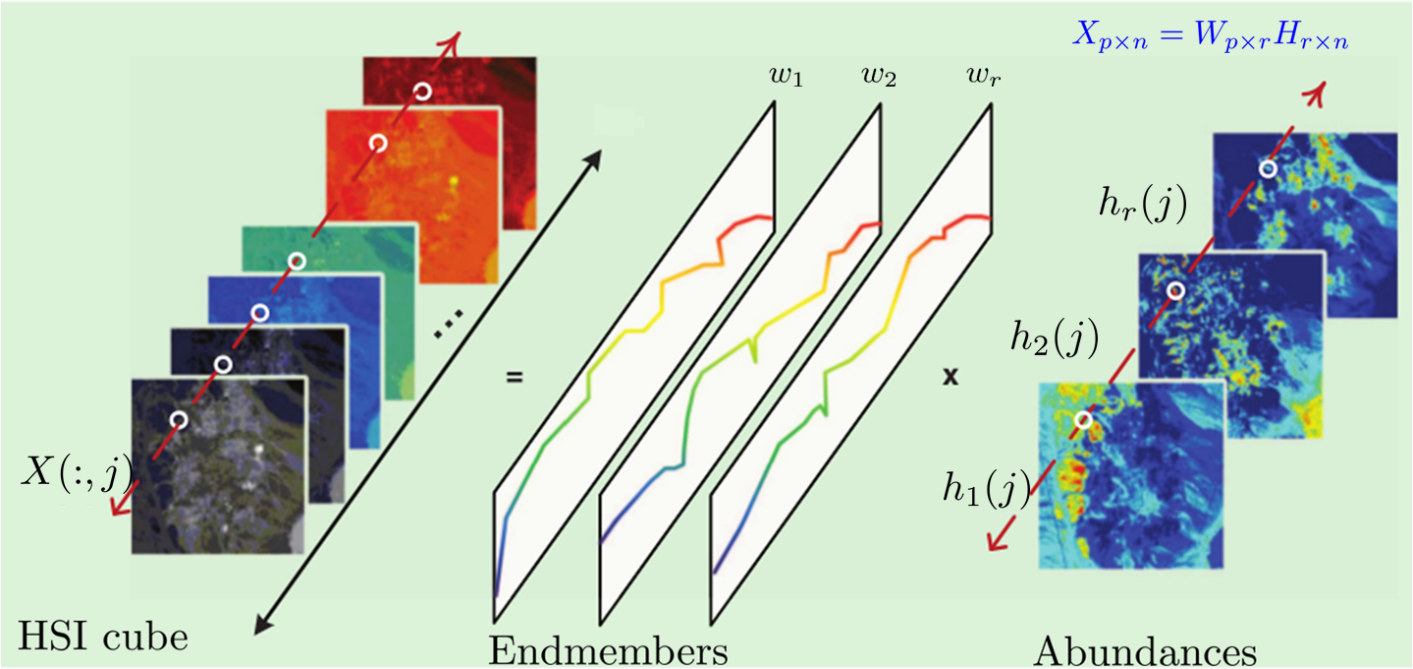

$$X(:,j) = \sum_{i=1:r} \mathbf{w}_i \cdot h_i(j)$$

Constraints:

- At pixel j we require $\sum_i h_i(j) = 1$.
- $W, H \geq 0$

Non-negative matrix factorization(NMF) [3]

- Low rank approximation of a matrix $X \in \mathbb{R}^{p \times n}$

$$X = WH \text{ which minimizes } \|X - WH\|_F^2$$

with $W \in \mathbb{R}^{p \times r}, H \in \mathbb{R}^{r \times n}$

- Separable NMF [4] : "Most" pixels are dominated mostly by one end-member. This is called the pure-pixel condition implies $X(:, j) = W(:, k)$ as opposed to mixed pixels where $X(:, j) = W * H(:, j)$.

Hierarchical rank-2 NMF clustering [6]

Starts with one cluster containing all pixels in image, At each step:

- $E_i = \|X(:, \mathcal{K}_i)\|_F^2 - \sigma_1^2(X(:, K_i))$
- Selects cluster i with largest approximation error E_i
- Splits selected cluster by rank-2 SVD
- Representative pure-pixel for a cluster are ones with minimal Mean removed spectral angle(MRSA) w.r.t leading eigen vector.
- Stop once r-clusters are reached.
- Non-negative least-sqaures to calculate endmembers

$r = 1, 5, 9, 13, 17, 21, 25, 29$

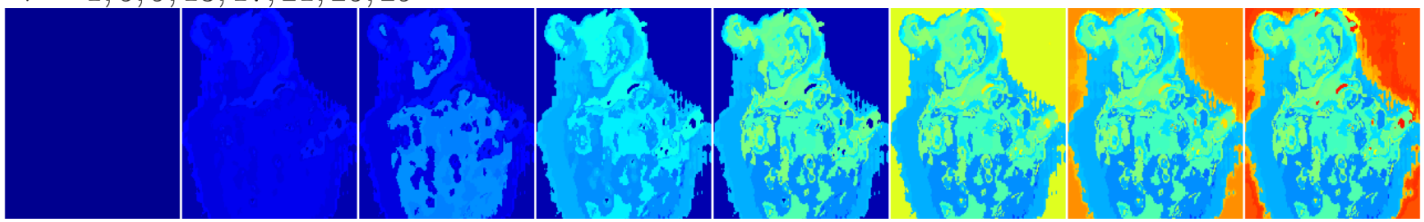

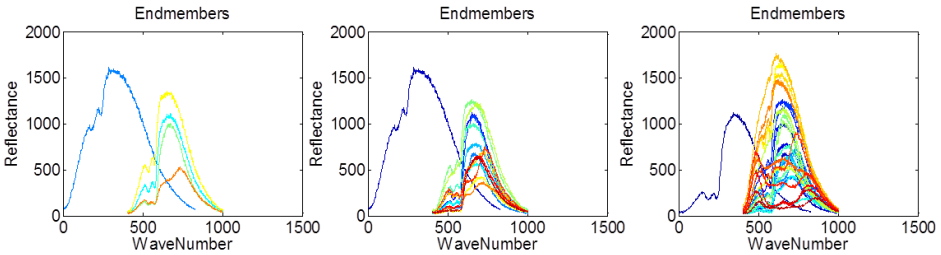

Endmembers at $r = 5, 15, 30$

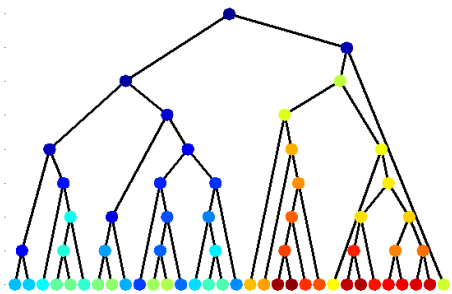

Cluster hierarchy

Training Set $(X_{\text{train}}, y_{\text{train}} = C_k)$

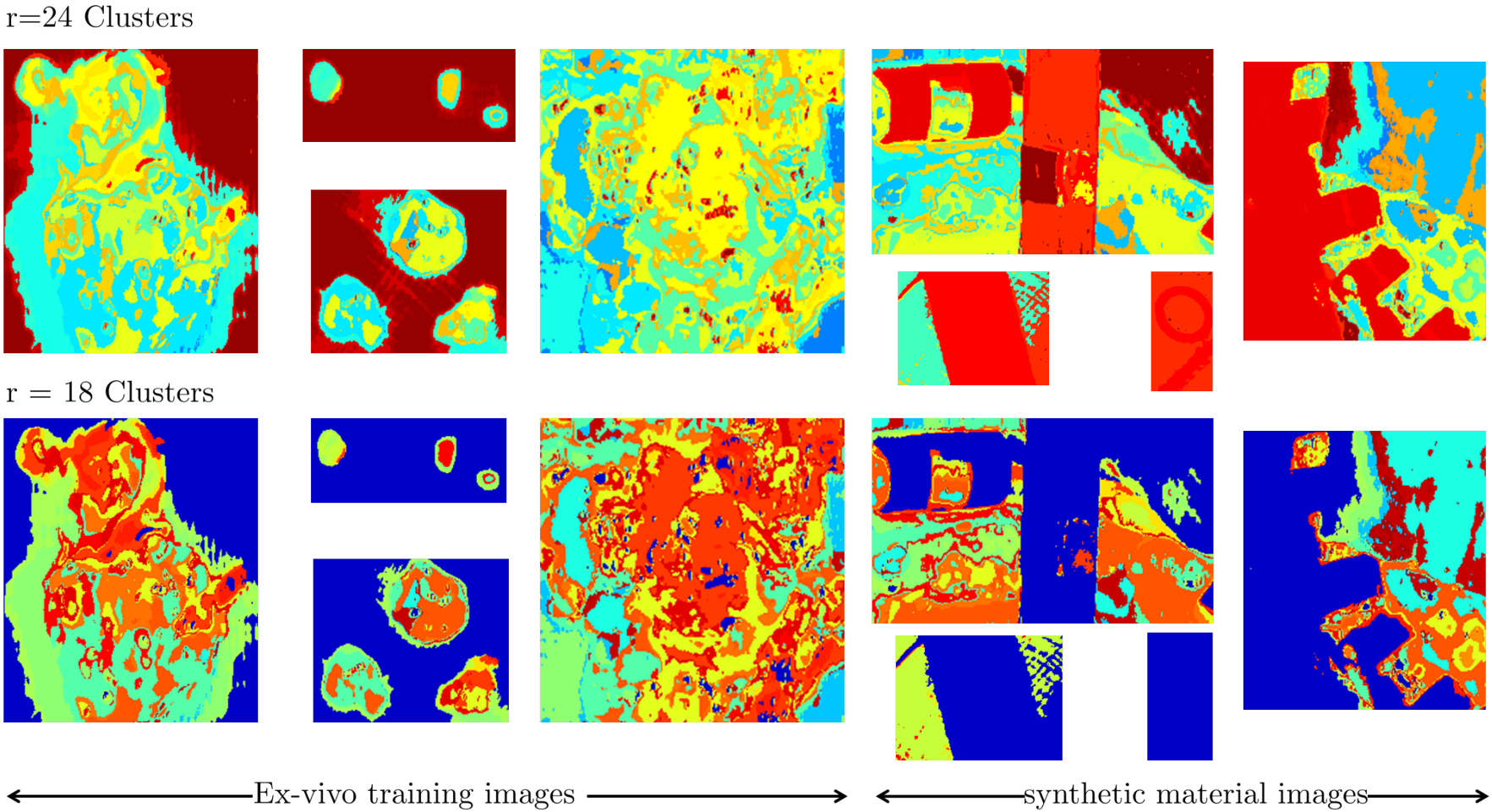

Figure : H2NMF clustering on the training set X_{train} which consists of input ex-vivo tumor tissue HSI cube and on materials. We in this case the ring on a cotton, and a cable in scene with open cranium and healthy tissues. This labeling with the corresponding HSI cubes serves as the training set for constructing the random forest classifier.

Classification of test images X_{test}

Test ex-vivo images (classification using labels at r=24 clusters)

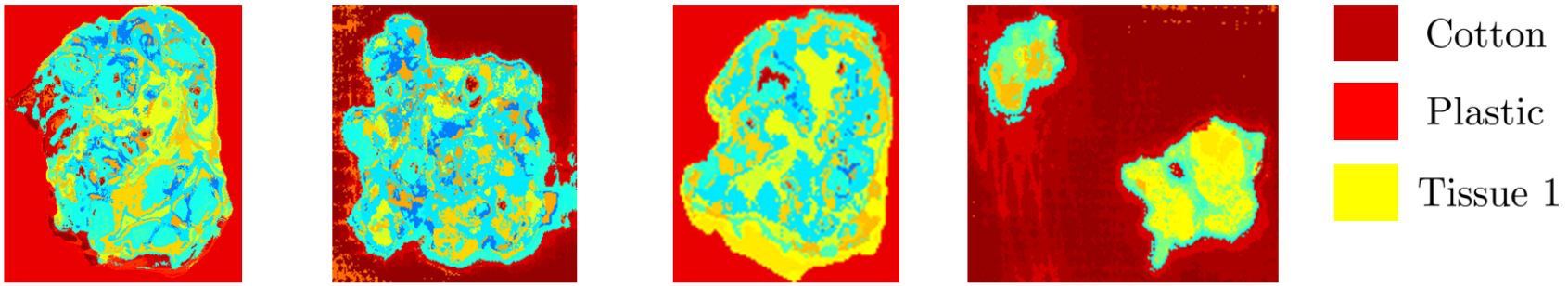

Test in-vivo images (classification using labels at r=24 clusters)

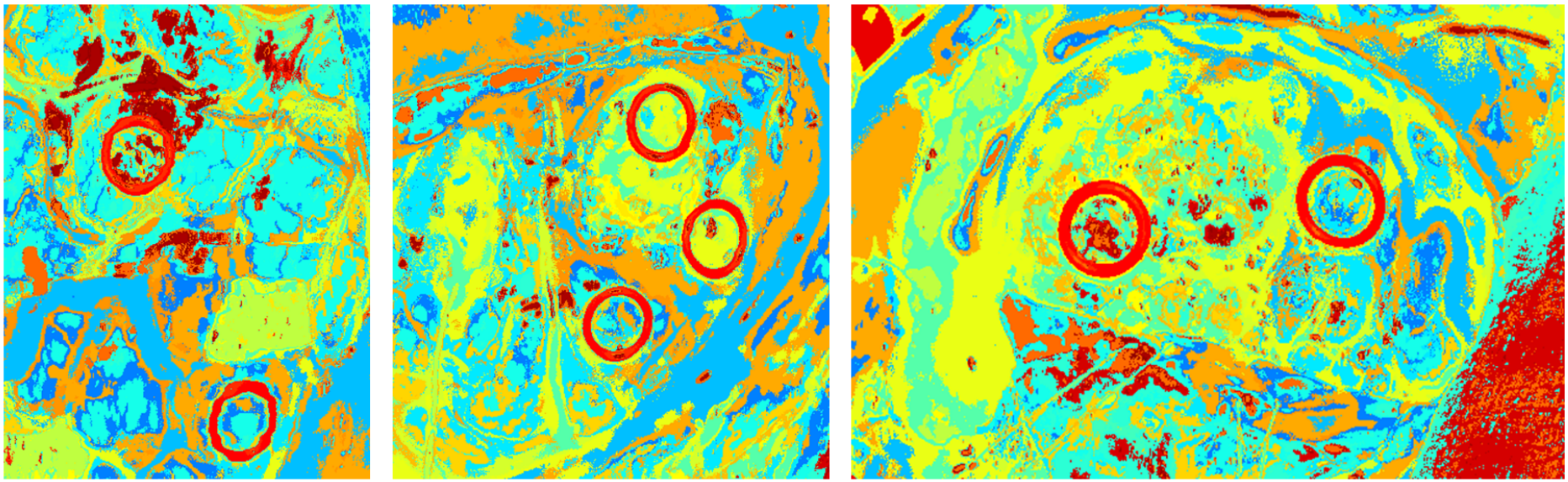

Classification of test images X_{test}

Test ex-vivo images (classification using labels at r=18 clusters)

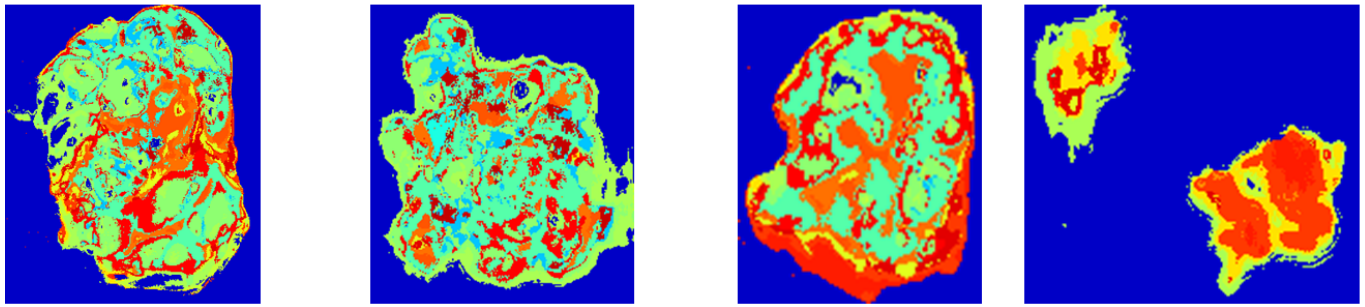

Test in-vivo images (classification using labels at r=18 clusters)

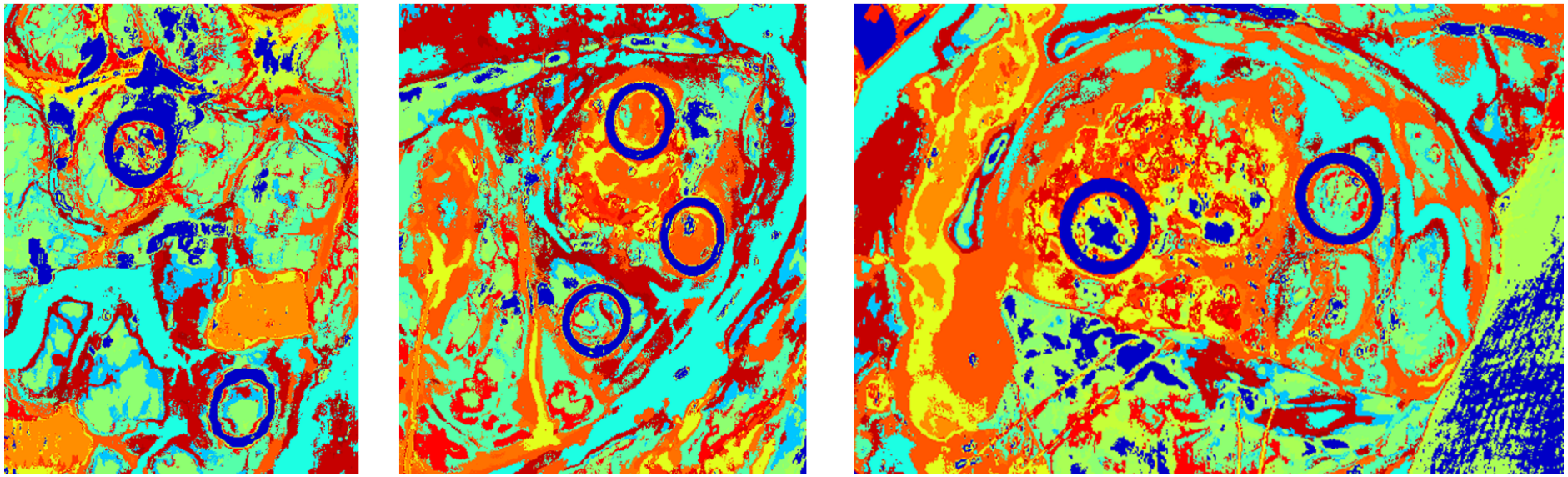

Specular Reflection

- HSI-pixel captures source lighting luminance instead of material reflectance due to total, partial or complex reflections from the thin films (specular) on tissue surface.
- This is not restricted to the optical range.

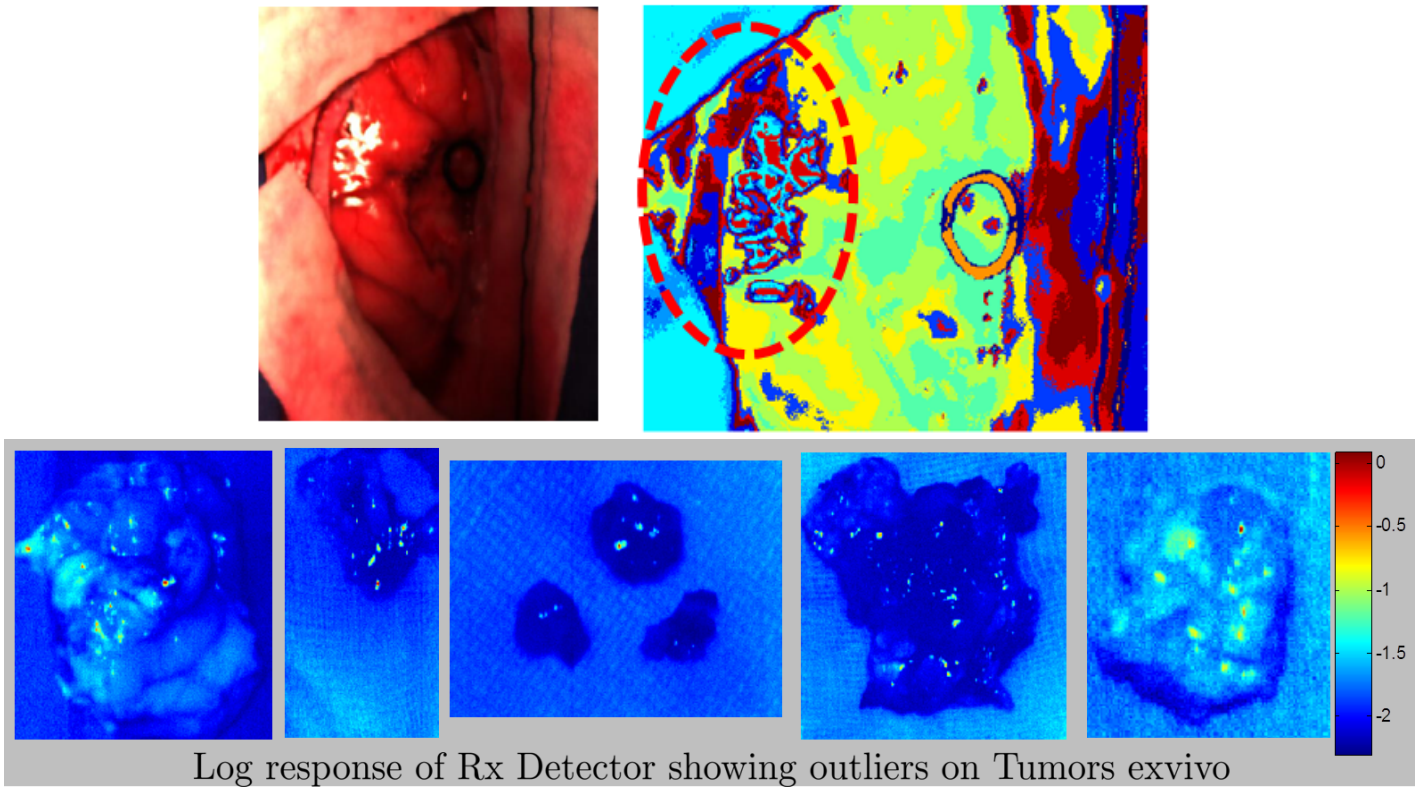

Log response of Rx Detector showing outliers on Tumors exvivo

Other Issues

Spectral similarity: Tumors Vs Normal Tissue :

- Differences between malignant and benign tissues in human breast tissues, have been attributed to the metabolic difference due to the presence of more oxy-hemoglobin, lipids and water [8]. Similar references for canine mammary tumors [12].
- Discriminatory feature : Slopes of spectrum (at pixel) between 510, 530 nm were most discriminatory for ovaries, while 630-900 nm for kidneys [13], [11].
- Due the lack of information during this study of the actual spectrum of tumor tissues we are unable to provide a a discriminatory feature, and thus supervised division of subspace.

Spectrum variation sources :

- Age, hormonal status, introduce high inter-patient variability in NIR absorption spectra and complicate diagnosis when only the magnitude of tissue absorption is used [2].
- Change in illumination and movement of push-broom sensor
- **Structure** : Solid tumors are composed of two distinct but interdependent compartments [5]: malignant cells themselves (parenchyma), the supporting connective tissue (stroma).
- Unlike the normal vasculature, tumor vessels are not arranged in a hierarchical pattern but are instead irregularly spaced and structurally heterogeneous.

Conclusion

- Spectral discrimination of tumor vs normal tissues not possible.
- Create (None yet) visual appearance models for tumors on tissue surface.
- Texture based features : granulometry?

Future work :

- Clearer problem formulation in terms of dimensionality reduction + spatial convolutional features [1].
- Use abundance maps for spatial features.
- Ongoing work on spatial interpolating markers by K-NN filtering.

The End

References I

[1] J. Bruna and S. Mallat. Invariant scattering convolution networks. *IEEE Trans. Pattern Anal. Mach. Intell.*, 35(8):1872–1886, aug 2013.

[2] A. Cerussi, N. Shah, D. Hsiang, A. Durkin, J. Butler, and B. J. Tromberg. In vivo absorption, scattering, and physiologic properties of 58 malignant breast tumors determined by broadband diffuse optical spectroscopy. *Journal of biomedical optics*, 11(4):044005–044005, 2006.

[3] A. Cichocki, R. Zdunek, A. H. Phan, and S.-i. Amari. *Nonnegative Matrix and Tensor Factorizations: Applications to Exploratory Multi-way Data Analysis and Blind Source Separation*. Wiley Publishing, 2009.

[4] D. Donoho and V. Stodden. When does non-negative matrix factorization give a correct decomposition into parts? In *Advances in neural information processing systems*, page None, 2003.

[5] H. F. Dvorak. How tumors make bad blood vessels and stroma. *The American journal of pathology*, 162(6):1747–1757, 2003.

[6] N. Gillis, D. Kuang, and H. Park. Hierarchical clustering of hyperspectral images using rank-two nonnegative matrix factorization. *IEEE T. Geoscience and Remote Sensing*, 53(4):2066–2078, 2015.

[7] B. R. Kiran, B. Stanciulescu, and J. Angulo. Unsupervised clustering of hyperspectral images of brain tissues by hierarchical non-negative matrix factorization. In *BIOIMAGING 2016*, volume 2, page 8. SCITEPRESS, 2016.

[8] S. Kukreti, A. E. Cerussi, W. Tanamai, D. Hsiang, B. J. Tromberg, and E. Gratton. Characterization of metabolic differences between benign and malignant tumors: High-spectral-resolution diffuse optical spectroscopy. *Radiology*, 254(1):277–284, 2010.

[9] W.-K. Ma, J. Bioucas-Dias, T.-H. Chan, N. Gillis, P. Gader, A. Plaza, A. Ambikapathi, and C.-Y. Chi. A signal processing perspective on hyperspectral unmixing: Insights from remote sensing. *Signal Processing Magazine, IEEE*, 31(1):67–81, Jan 2014.

[10] D. Manolakis and G. Shaw. Detection algorithms for hyperspectral imaging applications. *Signal Processing Magazine, IEEE*, 19(1):29–43, 2002.

[11] D. L. Peswani. *Detection of Positive Cancer Margins Intra-operatively During Nephrectomy and Prostatectomy Using Optical Reflectance Spectroscopy*. ProQuest, 2007.

References II

[12] A. Sahu, C. McGoverin, N. Pleshko, K. Sorenmo, and C.-H. Won. Hyperspectral imaging system to discern malignant and benign canine mammary tumors. In *SPIE Defense, Security, and Sensing*, pages 87190W–87190W. International Society for Optics and Photonics, 2013.

[13] U. Utzinger, M. Brewer, E. Silva, D. Gershenson, R. C. Blast, M. Follen, and R. Richards-Kortum. Reflectance spectroscopy for in vivo characterization of ovarian tissue. *Lasers in surgery and medicine*, 28(1):56–66, 2001.

H2NMF Algorithm [6]

- $X_{\text{train}} = \{I_j\} \cup \{E_i\}, i, j \in I \times J$
- I, J are the number of in-vivo and ex-vivo operations
- $E(i) = \sigma_1^2(X(:, \mathcal{K}_i^1)) + \sigma_1^2(X(:, \mathcal{K}_i^2)) - \sigma_1^2(X(:, K_i))$

Input: Input training set $X_{\text{train}} \in \mathbb{R}_+^{p \times n}$
Output: Set of disjoint clusters $\mathcal{K}_i, 1 \leq i \leq r$ with $\cup_i \mathcal{K}_i = (1, 2, ..., n)$

Initialize $\mathcal{K}_1 \leftarrow \{1, 2, ..., n\}$ and $\mathcal{K}_i \leftarrow \emptyset, k \leftarrow 1$ for $2 \leq i \leq r$
Initialize Clusters $(\mathcal{K}_1^1, \mathcal{K}_1^2) \leftarrow \text{splitting}(X_{\text{train}}, \mathcal{K}_1)$
while $k < r$ **do**
    $j \leftarrow$ cluster with largest error E
    $\mathcal{K}_j^1, \mathcal{K}_j^2 \leftarrow \text{splitting}(X, \mathcal{K}_j)$
    $\mathcal{K}_j \leftarrow, \mathcal{K}_k \leftarrow \mathcal{K}_j^2$
    $k \leftarrow k + 1$

Splitting

Input: Ex-vivo Cubes $X \in \mathbb{R}_{+}^{p \times m}$, $\mathcal{K} \subset \{1, 2, ...n\}$

Output: $\mathcal{K}^1, \mathcal{K}^1$ split cluster indices, $\mathcal{K} = \mathcal{K}^1 \cup \mathcal{K}^2$

1 $[W, H] = \text{rank2NMF}(X(:, \mathcal{K}))$ `/* Projection onto 2-d cone */`

2 $x(i) = \frac{H(1,i)}{H(1,i)+H(2,i)}$

3 Compute split parameter δ^*

4 $\mathcal{K}^1 = \{\mathcal{K}(i) | x(i) \geq \delta^*\}$

5 $\mathcal{K}^2 = \{\mathcal{K}(i) | x(i) < \delta^*\}$

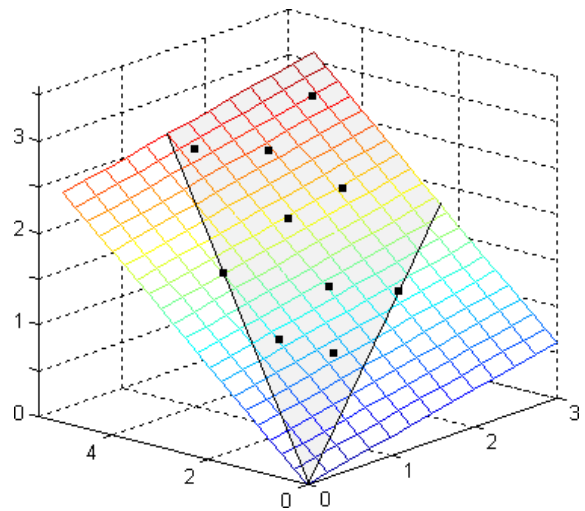

The 2-d cone on to which all columns of the input matrix are projected (figure repeated from [6]. On this cone δ^* decides the binary cluster. δ is chosen to trade-off between uniformity of cluster size and homogenity of clusters.

H2NMF Algorithm [6]

- Each splitting step produces one new endmember
- Leaves are Rank-1 submatrices containing "pure" pixels.
- Endmembers are calculated by calculating best rank-1 approximation $X(:, \mathcal{K}) = u_k v_k^T$ (by approx. svd)
- Representative pure-pixels are ones with minimal Mean removed spectral angle(MRSA) w.r.t u_k

$$\phi(\mathbf{x}, \mathbf{y}) = \frac{1}{\pi} \arccos\left(\frac{(x-\bar{x})^T(y-\bar{y})}{\|x-\bar{x}\|^2\|y-\bar{y}\|^2}\right) \in [0, 1]$$

- Abundances : by Non-negative least squares (NNLS).

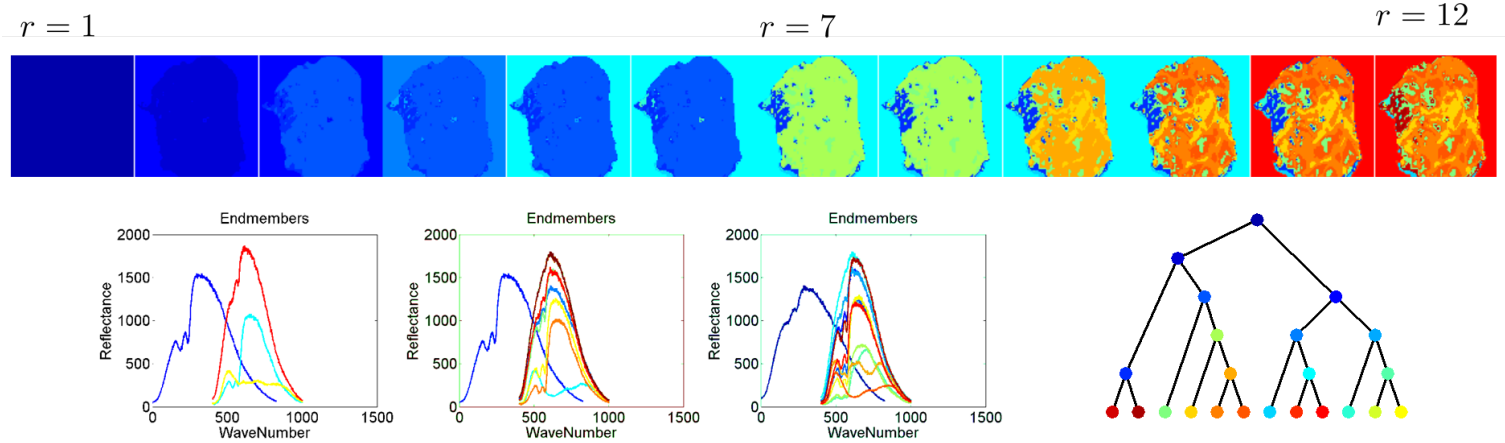

Unsupervised Clustering

- Progressively divide pixels until r-leaves with minimal approximation error are obtained.
- Subspace tree is used to train a Random forest with cluster centers to provide robustness to variation in centroids.
- BIOIMAGING 2016 [7].

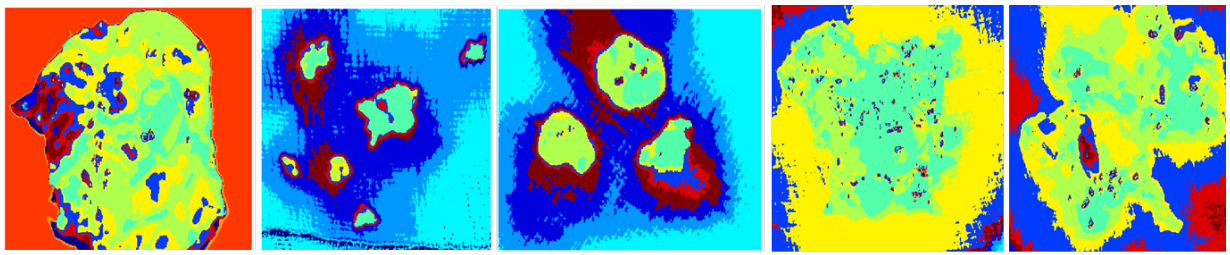

Ex vivo tumor cubes

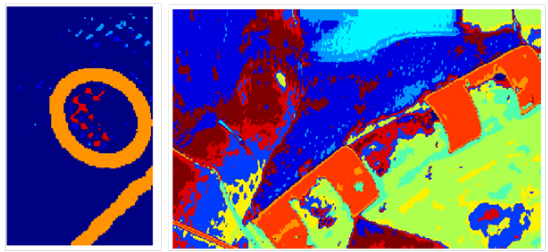

Material cubes

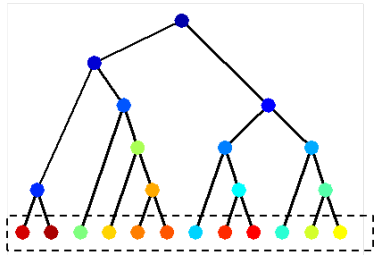

Subspace cluster Tree

Figure : H2NMF Clustering at level $r = 12$.

Clustering Results

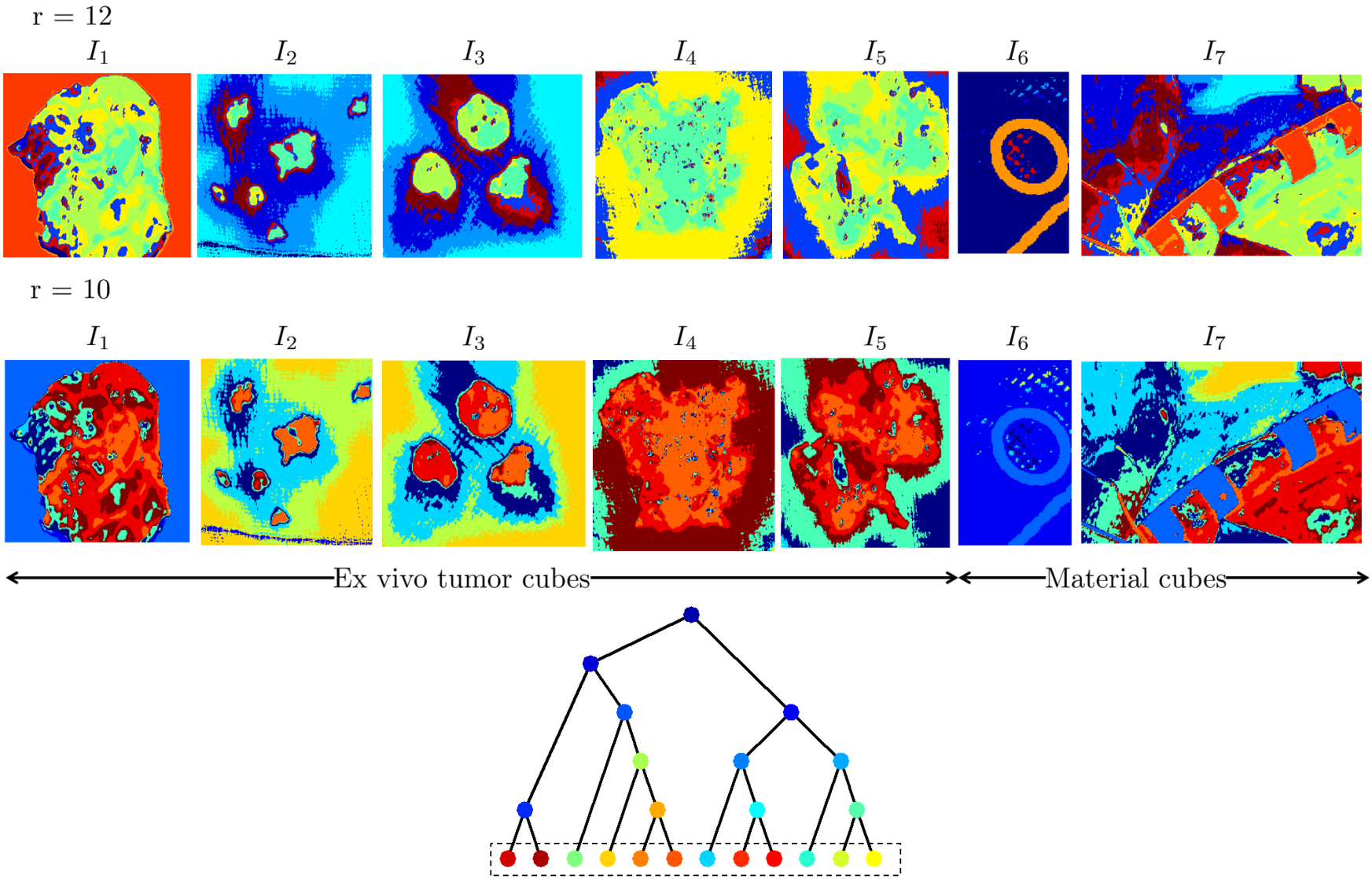

Figure : Two different levels of clustering.

In-vivo and Ex-vivo Images

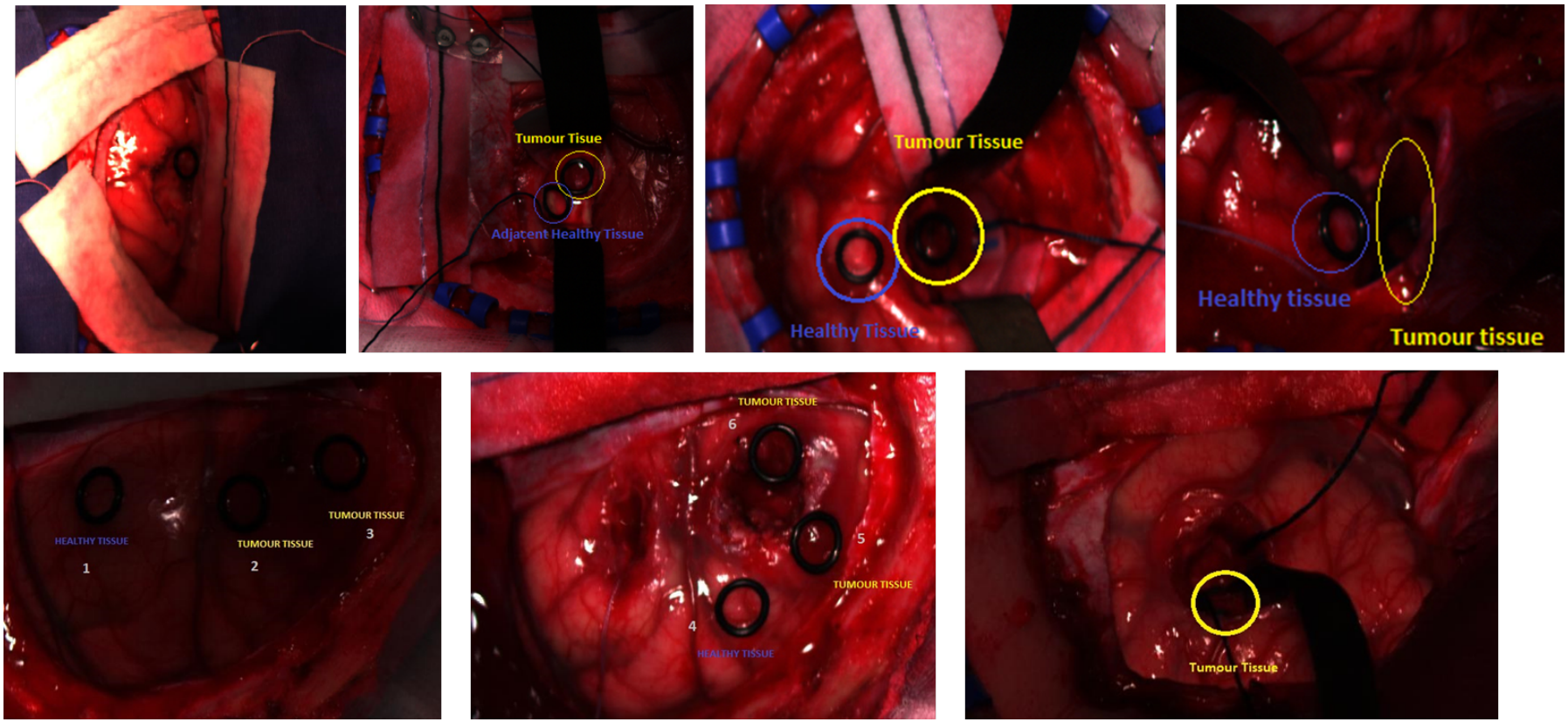

Figure : In-vivo scenes with their respective markers pair of synthetic rings. These rings are identifiable easily with the H2NMF clustering. One ring is assure to surround a cancerous tissue, while the other a healthy one. In such tests one still has no accurate estimate of the depth of penetration of VNIR rays as well as the fact that the tissue on the surface is cancerous. This is tough to ensure during critical surgeries.